Impacts on cloud radiative effects induced by coexisting aerosols converted from international shipping and maritime DMS emissions

Qinjian Jin[1], Benjamin S. Grandey[2], Daniel Rothenberg[1], Alexander Avramov[1†], Chien Wang[1,2]

[1]Center for Global Change Science, Massachusetts Institute of Technology, Cambridge, Massachusetts, USA.
[2]Center for Environmental Sensing and Modelling, Singapore–MIT Alliance for Research and Technology, Singapore.
† Now at Department of Environmental Science, Emory University, Atlanta, Georgia, USA.

Correspondence to: Qinjian Jin (jqj@mit.edu)

Abstract. International shipping emissions (ISE), particularly sulfur dioxide, can influence the global radiation budget by interacting with clouds and radiation after being oxidized into sulfate aerosols. A better understanding of the uncertainties in estimating the cloud radiative effects (CRE) of ISE is of great importance in climate science. Many international shipping tracks cover oceans with substantial natural dimethyl sulfide (DMS) emissions. The interplay between these two major aerosol sources on cloud radiative effects over vast oceanic regions with relatively low aerosol concentration is an intriguing yet poorly addressed issue confounding estimation of the cloud radiative effects of ISE. Using an Earth system model including two aerosol modules with different aerosol mixing configurations, we derive a significant global net CRE of ISE (-0.153 W m^{-2} with standard error of ±0.004 W m^{-2}) when using emissions consistent with current ship emission regulations. This global net CRE would become much weaker and actually insignificant (-0.001 W m^{-2} standard error of ±0.007 W m^{-2}) if a more stringent regulation were adopted. We then reveal that the ISE-induced CRE would achieve a significant enhancement when lower DMS emission is prescribed in the simulations, owing to the sub-linear relationship between aerosol concentration and cloud response. In addition, this study also demonstrates that the representation of certain aerosol processes, such as mixing states, can influence the magnitude and pattern of the ISE-induced CRE. These findings suggest a re-evaluation of the ISE-induced CRE with consideration of DMS variability.

1 Introduction

Marine stratiform clouds have a strong cooling effect on the climate system. They cover about 30% of the global ocean surface (Warren et al., 1988), and can reflect more solar radiation back to space than the dark ocean surface at cloud-free conditions. On the other hand, low-altitude marine stratiform clouds form and develop near to the ocean surface (only several degrees cooler than ocean surface) and thus have limited impacts on the longwave radiation balance (Klein and Hartmann, 1993). Therefore, the annual-mean net radiative effect of cloud at the top of the atmosphere (TOA) is negative (i.e., cooling) and can be up to -20 W m^{-2} on the global scale (Boucher et al., 2013). Consequently, even a few percent change in marine stratocumulus cloud cover can double or offset the anthropogenic global warming due to greenhouse gases.

Sulfate aerosols are efficient cloud condensation nuclei and control the formation of marine clouds and their micro- and macro-physical properties (McCoy et al., 2015). The international shipping-emitted sulfur dioxide from combustion of heavy fossil oil (Figure 1) can be oxidized to sulfate aerosols that can increase cloud droplet number concentrations, cloud liquid water path, and planetary albedo, resulting in more solar radiation being reflected back to space, exerting a cooling effect on the climate system (Capaldo et al., 1999; Devasthale et al., 2006; Lauer et al., 2007; Lauer et al., 2009). Although international shipping emissions (ISE) contribute only about 5% (5.4 Tg S yr^{-1}) to the total anthropogenic sulfur emissions (Corbett and Koehler, 2003; Endresen et al., 2005; Klimont et al., 2013), they dominate the sulfur concentration across much of the ocean,

37 such as the North Pacific Ocean (NPO) and the North Atlantic Ocean (NAO), as shown in Figure 2. Therefore, the radiative

38 impact of the ISE via perturbing marine stratocumulus clouds could be large—especially because marine stratocumulus clouds

39 are often collocated with busy shipping lanes (Neubauer et al., 2014). Note that although ISE also contain significant amount of

40 black carbon and organic carbon aerosols, since this study mainly focuses on aerosol induced CRE instead of aerosol direct

41 radiative effect, we focus on only primary and secondary sulfate aerosols due to their much higher hygroscopicity than those of

42 black carbon and organic carbon aerosols (Pringle et al., 2010),

43   The estimated global annual mean of the ISE-induced net cloud radiative effect (CRE) at TOA has large uncertainties

44 due to the complication in simulating clouds and aerosol–cloud interactions, ranging from −0.60 to −0.07 W m^{-2} (Capaldo et al.,

45 1999; Lauer et al., 2007; Eyring et al., 2010; Righi et al., 2011; Peters et al., 2012; Partanen et al., 2013; Peters et al., 2013).

46 Compared with net CRE, the net direct radiative effect (DRE) of shipping emissions is much weaker, with a magnitude of only

47 −0.08 to −0.01 W m^{-2}, approximately one tenth of the former (Endresen et al., 2003; Schreier et al., 2007; Eyring et al., 2010).

48   Besides shipping-emitted sulfur compounds, oceanic phytoplankton-derived dimethyl sulfide (DMS) is another

49 significant component in the atmospheric sulfur cycle over oceans (Grandey and Wang, 2015; Mahajan et al., 2015; McCoy et

50 al., 2015; Tesdal et al., 2016). DMS can be oxidized by hydroxyl radical or nitrate radical to produce sulfur dioxide and finally

51 converted to sulfate aerosols (Boucher et al., 2003). The global total DMS emission is estimated to range from 8 to 51 Tg S yr^{-1}

52 based on model simulation (Quinn et al., 1993; Dentener et al., 2006); this uncertainty range is itself substantially larger than the

53 total sulfur emissions from shipping. The global annual mean of the DMS-induced net CRE at TOA ranges from −2.03 to −1.49

54 W m^{-2} determined by DMS climatology (Gunson et al., 2006; Thomas et al., 2010; Mahajan et al., 2015).

55   Most of the aforementioned studies addressed separately the impacts on CRE of shipping and DMS emissions, largely

56 ignoring the potential nonlinearity in the response of cloud radiative effects to aerosol variations when these sulfate aerosols

57 from two different sources often collocate in the marine atmosphere, such as NPO and NAO (Figure 1). The nonlinearity

58 between DMS emission and the associated CRE was studied previously without taking into account the shipping emissions

59 (Pandis et al., 1994; Russell et al., 1994; Gunson et al., 2006; Thomas et al., 2011). Here, to evaluate the CRE induced by both

60 ISE and DMS emissions with a consideration of their interactions, we selected three regions for detailed analysis: the NPO and

61 NAO where the ISE dominate the concentrations of sulfur dioxide and sulfate aerosols, and the Southern Ocean where DMS is

62 the dominant source (Figure 2).

63   This study employs an Earth system model including an interactive aerosol model that simultaneously resolves both

64 external and internal mixtures of sulfate, black carbon, and organic carbon aerosols. Aerosol mixing in this way can resolve

65 aerosol activation process more realistically than either mixing all aerosol species internally or ignoring any mixing at all. By

66 comparing the results with the default aerosol scheme that assumes internal mixing, we also quantify the impacts of various

67 assumptions of aerosol mixing states on estimates of the CRE of ISE and DMS emissions. We further quantify the ISE-induced

68 CRE based on various regulations of the International Maritime Organization (IMO) on the fuel sulfur content. Therefore, our

69 findings have important implications for policy makers and future estimates of CRE induced by both ISE and DMS emissions.

70 **2 Methods**

71 **2.1 Climate model**

72   The Community Earth System Model version 1.2.2 (CESM1.2.2) is configured with the Community Atmosphere Model

73 version 5.3 (CAM5.3). CAM5.3 includes a modal aerosol model with an option of 3 or 7 lognormal distributions of aerosol size

74 (MAM3 or MAM7). In this study, a new modal aerosol model—the two-Moment, Multi-Modal, Mixing-state resolving Aerosol

75 model for Research of Climate (MARC; version 1.0.3 here) (Kim et al., 2008; Kim et al., 2014; Rothenberg and Wang, 2016,

76 2017; Grandey et al., 2018) is introduced and used to evaluate both the DRE and CRE of ISE. The details of MARC are

77 described below. Aerosol DRE are represented by coupling between aerosols and radiation. Aerosol CRE are included by

78 activating aerosols to work as cloud condensation nuclei and ice nuclei in the stratiform clouds (Morrison and Gettelman, 2008;

79 Gettelman et al., 2010). Parameterization of aerosol activation is based on particle size and hygroscopicity of aerosols. Similar to

80 other climate models, CAM5 does not directly include aerosol's influence through microphysics on convective clouds, but it

81 allows aerosols to influence convective clouds indirectly, such as by aerosol's effect on circulation, surface evapotranspiration

82 and so on.

83 **2.2 MAM3**

84 The default aerosol scheme in CESM 1.2.2, MAM3, has three modes, each with a lognormal size distribution: Aitken,

85 accumulation, and coarse. Various aerosol species are internally mixed within each mode. Aitken mode is a mixture of sulfate,

86 secondary organic carbon and sea salt; accumulation mode is mixture of sulfate, black carbon, primary organic carbon,

87 secondary organic carbon, dust, and sea salt; coarse mode is a mixture of dust, sea salt, and sulfate (Liu et al., 2012). MAM3

88 tracks both the mass concentration and the number concentration of each aerosol mode.

89 **2.3 MARC**

90 MARC uses seven modes with different lognormal size distribution to represent the population of sulfate and

91 carbonaceous aerosols: three modes for pure sulfate (nucleation or NUC, Aitken or AIT, and accumulation or ACC), one each

92 for pure black carbon (BC) and pure organic carbon (OC), one mixture of BC–sulfate in core-shell structure (MBS), and one

93 mixture of OC–sulfate (internal mixture; MOS). MARC predicts total particle mass and number concentrations while assuming

94 the standard deviation within each of the seven modes to define at any given time the lognormal distribution of particle size. In

95 addition, carbonaceous mass concentrations inside MBS and MOS are also predicted to allow the mass ratios between sulfate

96 and carbonaceous compositions to evolve over time, changing the optical and chemical properties of the mixed aerosols. The

97 emissions of mineral dust and sea salt that MARC uses are calculated by the land surface model and atmosphere model,

98 respectively (Mahowald et al., 2006; Albani et al., 2014; Scanza et al., 2015). Mineral dust and sea salt are each represented by

99 four bins with fixed sizes in MARC. For details of MARC aerosol mode size distribution and chemical parameters, please refer

100 to Rothenberg and Wang (2017). Note that in MARC model, gas-phase sulfur compounds can be oxidized in both gaseous and

101 aqueous phase to form sulfate that could enter aerosol phase in several pathways: (1) aerosol nucleation to form new nucleation

102 mode sulfate aerosols; (2) condensation of gaseous sulfuric acid on both external sulfate and carbonaceous aerosols (the latter

103 specifically ages carbonaceous aerosols to form sulfate-carbonaceous aerosol mixtures); and (3) evaporation of cloud and rain

104 drops that resuspends aqueous sulfate to accumulation mode sulfate aerosol (Kim et al., 2008; Grandey et al., 2018; Rothenberg

105 et al., 2018).

106 **2.4 Difference between MARC and MAM3**

107 The most fundamental difference between MARC and MAM is that MARC includes both external and internal mixtures of

108 aerosols in fifteen modes while MAM treats all aerosols as internal mixtures in three modes. As a result, the processes of many

109 aerosol microphysical processes including gaseous condensation, new particle formation, and nucleation scavenging differ

110 between these two models (Kim et al., 2008; Grandey et al., 2018; Rothenberg et al., 2018). "For instance, aerosol activation or

111 nucleation scavenging in MARC and MAM3 is calculated based on competition for water vapor among various types (or modes)

112 of aerosols with different hygroscopicity. In this case, external sulfate modes and the mixture of BC and sulfate (MBS) with BC
113 as core and sulfate as shell would have the same hygroscopicity as sulfate, while external BC and OC would have much lower
114 hygroscopic values. Whereas, MAM calculates this process based on the volume weighted hygroscopicity of each mode based
115 on all the aerosol constitutions within the mode. In that case, the change of individual aerosol species would not influence much
116 the number of activated aerosol substantially" (Rothenberg et al., 2018).

117 **2.5 Radiation diagnostics**

118   In the diagnostic mode of CESM-MARC, the DRE are diagnosed by calling the radiation scheme three times in each
119 radiation time step. The first call does not include any aerosols, providing "clean-sky" diagnostics (Ghan, 2013). The second call
120 includes only mineral dust and sea salt aerosols. The third call includes all aerosols. The first and third call are diagnostic, i.e. the
121 radiation budget calculated from these two calls are only used to as model output, therefore they do not influence model
122 integration in the next time step; while the second call is prognostic, i.e., the radiation budget from this call is passed to other
123 model schemes to calculate associated model variables, such as temperature, surface evaporation and so on. Therefore, DRE of
124 only dust and sea salt aerosols are prognostic while all other aerosols including ISE are diagnostic. Note that all radiation
125 variables calculated in these three calls are stored in the model history files for further analyses. In the complimentary MAM3
126 simulations, the first radiation call (prognostic) includes all aerosols while the second call is a "clean-sky" diagnostic call,
127 excluding all aerosols.
128   The DRE of aerosols is calculated by subtracting the TOA radiation in the "clean-sky" call (no direct aerosol–radiation
129 interaction) from that in the call that includes all aerosols. The CRE is calculated by subtracting the TOA radiation at clear-sky
130 from that at all-sky in the "clean-sky" call (Ghan, 2013). The calculation of the DRE and CRE of ISE takes a further step—
131 subtracting the DRE and CRE in simulation without ISE from that with ISE. In this way, the DRE and CRE of ISE can be
132 isolated and evaluated separately. Note that all radiative effects are calculated at TOA.

133 **2.6 Experimental design**

134   Three groups of simulations are designed to evaluate: (*a*) the DRE and CRE of ISE, and (*b*) the sensitivity of the ISE-
135 induced CRE to both DMS emissions and aerosol mixing assumptions. CAM5 was run at a horizontal resolution of 1.875°×2.5°
136 and 30 vertical layers with sea surface temperature (SST), sea ice, greenhouse gas concentrations prescribed at the level of year
137 2000. The aerosol emissions in year-2000 were used except for modified shipping and DMS emissions. The DMS emission is
138 prescribed with a global annual average of 18.2 Tg S yr^{-1} in DMS reference simulations (Dentener et al., 2006). Each simulation
139 runs for 32 years driven by 12-month cyclic climatological sea surface temperature, with the first 2 years discarded as spin up.
140 Since the SSTs were prescribed, a 2-year period of spin up should be enough for aerosol concentrations and other model
141 components to reach an equilibrium state (e.g., Righi et al., 2011).
142   The first group uses CESM-MARC and includes four simulations, which share the same DMS reference emissions
143 (*DMSRef*) while differing in four various ISE of sulfur compounds (sulfur dioxide and sulfate) (Table 1). *ShipZero_DMSRef*
144 simulation is integrated excluding all aerosol and aerosol precursor emissions from ISE, i.e., sulfur dioxide, sulfate aerosol,
145 organic carbon aerosol, and black carbon aerosol. The other three simulations—*ShipLow_DMSRef*, *ShipRef_DMSRef*, and
146 *ShipHigh_DMSRef*—include the standard emissions of carbonaceous aerosols (e.g., BC and OC) while use three various
147 emission scenarios of sulfur compounds from ISE. The three emission scenarios are based on the assumptions of sulfur content
148 of the heavy fuel oils for ocean-going ships. Currently, the average sulfur content is 2.7% (Corbett and Koehler, 2003; Endresen
149 et al., 2005), which is equivalent to about 5.4 Tg S year^{-1}, referred to as *ShipRef*. On the other hand, as of 2013 the high sulfur

150 fuel oil that has 3.5% sulfur content continued to be permitted outside the Emission Control Areas (Lauer et al., 2009; Winebrake

151 et al., 2009), referred to as *ShipHigh*. However, the IMO has planned to lower the sulfur content to 0.5% outside the Emission

152 Control Areas (Winebrake et al., 2009; Notteboom, 2010; International Maritime Organization, 2016) after 2020, referred to as

153 *ShipLow*. In *ShipLow* and *ShipHigh*, the total global sulfur shipping emissions are 1.0 and 7.2 Tg S year^{-1}, respectively. These

154 numbers related to annual sulfur emissions are generally estimated based on the total amount of heavy fuel burnt by ships and the

155 associated emission rates, whose uncertainties were addressed by Peters et al. (2012). The differences between these three and

156 the zero shipping emission scenarios represent how various regulations on marine fuel influence the ISE-induced CRE.

157   The second group also uses CESM-MARC and is comprised of three pairs of simulations: (*ShipRef_DMSZero*,

158 *ShipZero_DMSZero*), (*ShipRef_DMSLow*, *ShipZero_DMSLow*), and (*ShipRef_DMSRef*, *ShipZero_DMSRef*). Note that the pair

159 of (*ShipRef_DMSRef*, *ShipZero_DMSRef*) simulations are also part of the first group. The annual emission of DMS is 18.2 Tg S

160 year^{-1} in the *DMSRef* simulations (Dentener et al., 2006; Liu et al., 2012), and half of that in the *DMSLow* simulations. DMS

161 emission is excluded in the *DMSZero* simulations. Each pair of the simulations include *ShipZero* and *ShipRef*, the difference of

162 which represents the ISE-induced impacts. The purposes of the *DMSZero* and *DMSLow* simulations are to quantify the

163 sensitivities of the ISE-induced CRE (i.e., the difference of CRE in each pair of simulations) to DMS emission and the associated

164 large uncertainty in DMS emission, respectively (Quinn et al., 1993; Dentener et al., 2006). DMS emission in the *DMSLow*

165 simulation is 9.1 Tg S year^{-1}, which is close to the lower boundary of DMS emission estimates, i.e., 8 Tg S year^{-1} (Quinn et al.,

166 1993). Such sensitivities are examined by calculating the differences among the three pairs of DMS simulations.

167   The third group is the same as the second, but using the default MAM3 aerosol module of CAM5.3 in CESM. The

168 purpose for designing the third group is to cross-validate the simulated DMS impacts on the ISE-induced CRE in the second

169 group. One bonus of the third group is to quantify the impacts of using different aerosol modules with different aerosol mixing

170 states on the simulated results. The anthropogenic emissions for MAM3, which are described by Liu et al. (2012), differ slightly

171 from those for MARC. All of the experiments are summarized in Table 1.

172 **3 Results**

173 **3.1 DRE of ISE**

174   The all-sky DRE of various aerosol species from ISE is diagnosed as the difference between ShipRef_DMSRef and

175 ShipZero_DMSRef and shown in Figure 3. The total ISE can cause a global negative (cooling) DRE of −23.5 mW m−2, with the

176 strongest negative (cooling) DRE in the areas with intense shipping tracks, such as mid-latitude areas in the Pacific Ocean and

177 Atlantic Ocean, South China Sea, North Indian Ocean, and the Red Sea. The sulfate aerosols in the accumulation mode (i.e.,

178 ACC) contribute 89% to the global total DRE, followed by MOS aerosols with a contribution of 22%. Note that OC and MBS

179 has a counteracting warming effect (Remember that all gas-phase and aerosol emissions from shipping have been removed in

180 ShipZero scenarios). The contributions of other aerosol species are very limited and their magnitudes are smaller than 6%. The

181 magnitude of the total cooling effect is within the range from −50 to −10 mW m−2 estimated in previous studies (Endresen et al.,

182 2003; Schreier et al., 2007). The meridional variations of global zonally-averaged total DRE show that the DRE has the strongest

183 cooling effect of −80 mW m−2 between 30°N and 40°N and becomes weaker towards both polar regions and can be ignored

184 beyond 45°S and 60°N. The all-sky DRE of total aerosols in ShipLow_DMSRef and ShipHigh_DMSRef have similar patterns to

185 those in ShipRef_DMSRef and have magnitudes of +1.0 and −33.0 mW m−2, respectively. All of the calculated global DRE

186 values except for BC are confident at the 90% level.

3.2 CRE of ISE under various shipping emission regulations

The CRE of ISE is much stronger than the DRE and shows different spatial patterns under various shipping emission regulations (Figure 4). At the reference level of shipping emissions (*ShipRef_DMSRef*), significant cooling CRE in SW is simulated in areas of intense shipping tracks, such as the mid-latitude Pacific Ocean and the Baffin Bay between Canada and Greenland, with a global average of −0.218 W m^{-2}. The LW CRE shows positive values in some small areas of high latitude, with a global average of +0.065 W m^{-2}. Consequently, the global net CRE (SW+LW) is −0.153 W m^{-2} with a similar spatial pattern to that of SW. At the high level of shipping emissions (*ShipHigh_DMSRef*), the CRE changes to −0.253, +0.073, −0.179 W m^{-2} for SW, LW, and net, respectively; more areas show significant changes than in *ShipRef_DMSRef*. Note that all of the above values are statistically significant above the 90% confidence level. However, at the low level of shipping emissions (*ShipLow_DMSRef*), fewer areas demonstrate significant changes than in *ShipRef_DMSRef* and *ShipHigh_DMSRef* and the global averages of the CRE are not significant at the 90% confidence level for SW and net. These results indicate that more stringent shipping emission regulation on sulfur content decided by the IMO to be applied after 2020 could effectively reduce or even largely eliminate the net CRE induced by ISE.

Further analyses demonstrate that the changes in CRE are caused by perturbations in both cloud water path (CWP; Figure S1) and column-integrated cloud droplet number concentrations (CDNC; Figure 5) induced by ISE. Figure S1 demonstrates significant increases in total CWP mainly over the NPO and NAO at the reference and high levels of ISE. The increases in total CWP is largely (87%) attributed to liquid CWP with the remaining contribution (13%) from ice CWP at the reference shipping emission level. Such increases in CWP could reflect more solar radiation to space and thus cause a cooling radiative effect at TOA, as shown in Figure 4. Note that very limited areas in North Pacific Ocean show significant increases in ice CWP, indicating that a small portion of surface shipping emissions could be vertically transported to very high altitude and form ice cloud. At the high level of shipping emissions, a larger increase in CWP is simulated, which is consistent with the cooler radiative effects. However, no significant changes are simulated in total, ice, or liquid CWP at the low level of shipping emissions. Associated with increases in CWP, the column-integrated cloud droplet number concentration (CNDC) also illustrates significant increases at all levels of shipping emission (Figure 5), which collocate with increases in CWP (Figure S1) and decrease in CRE (Figure 4) over the NPO and NAO. The sulfate aerosols from shipping emissions are highly efficient cloud condensation nuclei (CCN) and thus can increase the CDNC, which in turn affects CWP. Note that cloud area fraction does not exhibit any significant changes due to shipping emissions (not shown).

3.3 CRE of ISE under various DMS emissions

The biogenic emissions of DMS over oceans can be oxidized to sulfates and compete against shipping emitted sulfates for CCN and thus could influence the ISE-induced CRE. We find that the shipping emission-induced CRE exhibits significantly different patterns and global averages at different emission levels of DMS (Figure 6). With DMS emissions ranging from the reference level to low and zero levels, the magnitude of the ISE-induced negative CRE at SW increases from 0.218 to 0.457 and 2.435 W m^{-2} on global scale, respectively; significant negative CRE is simulated over more areas in the SO. It is worth noting that the ISE-induced CRE can reach up to −6 W m^{-2} when DMS emission is turned off, such as over NPO and NAO, which is a very large negative forcing even on the local scale. Since there are no comparable values in the literature, this large negative forcing warrants a detailed evaluation in future studies using different climate models. For CRE at LW, more areas with significant warming are seen in the SO, NPO, and NAO, with the global averages change from +0.065 to +0.073 and +0.253 W m^{-2} when DMS emissions changes from the reference to low and zero levels, respectively. For net CRE, it shares the similar features with those at SW, but with smaller magnitudes.

The DMS emissions influence the ISE-induced CRE by perturbing the ISE-induced changes in CWP and column-integrated CDNC (Figures S2 and 7). The shipping emission-induced changes in the total and liquid CWP increase as DMS emission decreases, particularly over the SO, the NPO, and the NAO, while no significant changes are simulated in the ice CWP. The increased CWP is closely associated with the increases in the column-integrated CDNC, which changes from 0.305×10^9 m^{-2} (2.5%, relative to climatological CDNC in the *ShipZero_DMSRef* simulation) to 0.476×10^9 m^{-2} (3.9%) and 0.999×10^9 m^{-2} (8.3%) on global scale as DMS emission decreases. These results imply that DMS emissions are the dominant sources of cloud seeds over remote oceans. The most prominent increases in CDNC are seen in the SO, NPO, and NAO. These results suggest important roles of DMS emissions playing in modulating the ISE-induced changes in cloud properties and radiation. Note that cloud area fraction does not exhibit any significant change (not shown).

As demonstrated in the above analysis, the impacts of DMS emissions on cloud response to shipping emissions are the most prominent over the SO, the NPO, and the NAO, so further analyses are performed over these three regions. Figure 8 shows cloud responses to shipping emission at different DMS emission levels over the three oceanic regions. Generally, cloud responses become weaker and weaker as DMS emission increases from zero (*DMSZero*) to low (*DMSLow*) and reference (*DMSRef*) level over all of the three regions. The most prominent change in cloud response is over the NPO, followed by the NAO and the SO, which is probably due to the higher contribution of shipping emission to the total sulfur dioxide and sulfate aerosols over the NPO than the NAO and the SO (Figure 2b and 2e). The removal of DMS emission (*DMSZero*) has a much stronger influence on cloud response to shipping emission than reducing DMS emission by half (*DMSLow*), indicating a strong non-linear competing effect for CCN between DMS and shipping emission.

3.4 CRE of DMS under various shipping emissions

Similar to DMS emissions' impacts on the ISE-induced CRE and cloud properties, ISE could also influence the DMS emission-induced CRE and cloud properties. Generally, stronger cooling net CRE (-7.518 vs. -5.611 W m^{-2}) induced by DMS emissions are seen when shipping emissions are absent, particularly in areas of intense shipping tracks, such as over the NPO and the NAO (Figure 9). Such a net cooling CRE is mainly the result of SW CRE. Stronger cooling CRE is associated with larger increases in liquid and total CWP (Figure S3) and column-integrated CDNC (Figure S4) in simulations without shipping emissions than those with shipping emissions.

It is worth pointing out that DMS emissions have significant warming CRE at LW, particularly over mid- and high-latitude regions in the Southern Hemisphere and high-latitude regions in the Northern Hemisphere regardless of the presence of shipping emissions (Figure 9). Such a warming CRE could be attributed to increases in total cloud area fraction, which is further attributed to increases in the middle and low cloud area fraction in the high-latitude regions in both hemispheres (Figure S5). Our results indicate that DMS is a significant source to CCN in the extremely clean polar regions in both hemispheres.

The area-averaged cloud responses over the SO, the NPO, and the NAO, to DMS emissions at different shipping emission levels are shown in Figure 10. Cloud responses to DMS are stronger over the SO than over the NPO and the NAO regardless of the presence of shipping emissions due to the fact that DMS and shipping emissions respectively dominate the sulfur concentrations over the SO, and the NPO and the NAO (Figure 2). Moreover, cloud responses to DMS emissions become much stronger over all of the three oceanic regions when shipping emissions have been removed. However, such changes in cloud responses to DMS due to removal of shipping emissions (i.e., the slopes of the curves) are stronger over the NPO and the NAO than over the SO, which is caused by very limited shipping emissions over the SO. These results again indicate a strong non-linear competing effect for CCN between DMS and shipping emission.

3.5 Impacts of choice of aerosol module on the results

Besides the impacts of various ISE regulations and DMS emissions on the ISE-induced CRE, various assumptions about the aerosol mixing states could also have an impact. Figure 11 shows the same results as Figure 6 but using the MAM3 aerosol module instead of MARC. At the reference level of DMS emissions (*DMSRef*), the ISE-induced CRE are generally stronger in MAM3 (SW: −0.319, LW: +0.064, and Net: −0.255 W m^{-2}; Figure 11) than in MARC for SW and net radiation (SW: −0.218, LW: +0.065, net: −0.153 W m^{-2}; Figure 6). More areas with significant cooling CRE are simulated in MAM3 than in MARC, particularly in the Atlantic Ocean, West Pacific Ocean, and North Indian Ocean. At the low level of DMS emissions (*DMSLow*), both the global averages and spatial patterns of the CRE in MAM3 are very similar to those in MARC. The two aerosol modules show the biggest differences in CRE when DMS emissions are excluded (*DMSZero*). MARC simulates strong ISE-induced CRE over tropical regions and the subtropical and mid-latitude areas of the SO, while MAM3 gives no significant CRE over these regions. Generally, the ISE-induced CRE is stronger in MARC than in MAM3 when DMS emissions are excluded. The associated changes in CDNC and CWP due to ISE illustrates similar patterns to changes in CRE (Figures S6 and S7). A possible reason for such differences is the various mixing assumptions about sulfate and sea salt aerosols in MARC (external mixing) versus in MAM3 (internal mixing). Interested readers are referred to Grandey et al. (2018) for discussion of the differing radiative effects produced by MARC and MAM. To track down all the possible reasons for the differences in the ISE-induced CRE between the two aerosol schemes, more detailed analyses on a long chain of processes related to both aerosols and clouds are required, as done by Peters et al. (2014), which is out of the scope of this study and warrants more studies in the future.

By comparing Figure 8 with Figure 12 we also observe significantly different impacts of DMS emissions on cloud response to shipping emissions (i.e., the slopes of these curves). MAM3 simulates a weaker impact of DMS emissions on cloud response to shipping emissions than MARC, indicating a weaker non-linear competing effect for CCN between DMS and shipping emissions in MAM3 than MARC.

4 Conclusions and Discussion

Aerosols from ISE could exert significant cooling on the Earth's climate system through aerosol–cloud and aerosol–radiation interactions. To reduce the pollution and climatic effects from this emission source, the IMO set various emission caps on sulfur content of marine fuel oil to be implemented in the future. Using a state-of-the-art climate model, we find that the newly proposed more stringent emission regulations of shipping emissions can effectively reduce the ISE-induced CRE. As demonstrated in our results, reducing sulfur contents from 3.5% to 2.7% and 0.5% could reduce both DRE (from −51.4 to −36.7 and −3.9 mW m^{-2}) and CRE (from −0.179 to −0.153 and −0.001 W m^{-2}) due to ISE, respectively. Although the ISE-induced CRE would be insignificant on a global scale if sulfur contents of ship fuels were reduced to 0.5%, over some regions significant CRE can still be detected—e.g., high latitude regions of the eastern Pacific Ocean. Therefore, implementation of cleaner fuels in shipping sector, such as natural gas, could be a potential solution for completely eliminating sulfate-induced CRE.

More importantly, we find that the magnitude and regional spatial pattern of the ISE-induced CRE are highly sensitive to natural DMS emissions. With DMS emissions reducing from 18.2 to 9.1 Tg S yr^{-1} and zero, the ISE-induced net CRE changes from −0.153 to −0.384 and −2.182 W m^{-2}, respectively. On the other hand, the DMS-induced net CRE changes from −5.611 to −7.518 W m^{-2} when shipping emissions at the reference level are removed in the simulations. It is worth noting that DMS is a significant source to CCN in the extremely clean polar regions in both hemispheres. The strong interactions of CRE between DMS and shipping emissions can be attributed to the nonlinearity in the responses of cloud processes to aerosols, particularly the

302 aerosol activation parameterizations (Abdul-Razzak et al., 1998). In a relatively clean environment, activated aerosol number

303 concentration increases as ambient aerosol number concentration increases until reaching a peak at a specific aerosol number

304 concentration, after which it decreases as ambient aerosol number concentration increases unless ambient vapor concentration is

305 drastically increased. In other words, the fraction of activated aerosols decreases as ambient aerosol concentration increases

306 (Figure S8). From the perspective of simulation, this nonlinearity in aerosol activation strongly suggests a reevaluation of CRE

307 induced by shipping and DMS emissions as well as a reevaluation of parameterizations of aerosols–cloud interactions in the

308 general circulation models. From the perspective of field measurements of aerosol–cloud relationships, it warrants careful

309 attention when selecting measurement locations—shipping emissions-related measurements should be collected along intense

310 shipping tracks while in areas with as little DMS emissions as possible to avoid contamination from DMS, and vice versa.

311 Moreover, locations containing both shipping and DMS emissions should also be identified and sampled, in order to investigate

312 non-linear interactions between the emissions.

313 Finally, we find that two different aerosol schemes, with different representations of aerosol mixing state, could produce

314 a large difference (about 67%) in the ISE-induced global CRE. Generally, MARC aerosol module shows stronger nonlinear

315 cloud response to DMS and shipping emissions than MAM3. Overall, numerical studies on the uncertainties in the shipping

316 emission-induced CRE due to various ISE regulations, aerosol interactions, and aerosol mixing states can provide useful

317 information for policy makers and have implications for future projections of anthropogenic climate change.

318 Besides the above-mentioned contributors to the uncertainty in estimating the CRE induced by shipping emissions,

319 spatial resolution of the model is another significant source of this uncertainty. Possner et al. (2016) found that the ship-induced

320 shortwave CRE could increase by a factor of two as model spatial resolution decreases from 1 km to 50 km. With higher spatial

321 resolution, models can resolve fine-scale dynamical processes and feedbacks, such as interaction between aerosol and cumulus

322 clouds (Malavelle et al., 2017). Though model resolution-induced uncertainty is not the focus of this study, it should be taken

323 into account when interpreting the spread of shipping-induced CRE in studies of multi-model comparison.

324 Though we employed a state-of-the-art climate model in this study, it is not without caveats, given that neither MARC

325 nor MAM (including both MAM3 and MAM7 in CAM5) aerosol modules treat nitrate aerosols because of the high

326 computational expense for related aerosol-gaseous chemistry and aerosol thermodynamics calculations (Liu et al., 2012). Lack of

327 treating nitrate aerosols could result in uncertainties in our results based on the fact that both mass of nitrate aerosols emitted

328 from international shipping (e.g., Righi et al., 2011) and their hygroscopicity values (e.g., Kawecki and Steiner, 2018) are very

329 similar to those of sulfate aerosols, and thus nitrate aerosols could have non-negligible competing effects on CRE with sulfate

330 aerosols. Despite that some of the results from this study could be used to qualitatively project the potential outcome, a

331 quantitative assessment should be facilitated to address this topic with an improved model.

341 **Conflict of interest**

342 The authors declare no competing interests.

343 **Data and code availability**

344 The MARC source code is available via https://github.mit.edu/marc/marc_cesm/ and also archived with DOI

345 10.5281/zenodo.1117370, along with documentation on how to install and run the model. The commit 23e08fe was used in this

346 study. All the analysis code and model output data analyzed are available via

347 https://drive.google.com/drive/folders/1GHjrpvO06mzC8iFyT0Eif0PRiI56cReV?usp=sharing.

348

349

350

351 <div align="center">**References**</div>

352

353 Abdul-Razzak, H., Ghan, S. J., and Rivera-Carpio, C.: A parameterization of aerosol activation - 1. Single aerosol type, J Geophys Res-Atmos,
354   103, 6123-6131, 1998.
355 Albani, S., Mahowald, N. M., Perry, A. T., Scanza, R. A., Zender, C. S., Heavens, N. G., Maggi, V., Kok, J. F., and Otto-Bliesner, B. L.:
356   Improved dust representation in the Community Atmosphere Model, J Adv Model Earth Sy, 6, 541-570, 2014.
357 Boucher, O., Moulin, C., Belviso, S., Aumont, O., Bopp, L., Cosme, E., von Kuhlmann, R., Lawrence, M. G., Pham, M., Reddy, M. S., Sciare,
358   J., and Venkataraman, C.: DMS atmospheric concentrations and sulphate aerosol indirect radiative forcing: a sensitivity study to the
359   DMS source representation and oxidation, Atmos Chem Phys, 3, 49-65, 2003.
360 Boucher, O., Randall, D., Artaxo, P., Bretherton, C., Feingold, G., Forster, P., Kerminen, V.-M., Kondo, Y., Liao, H., Lohmann, U., Rasch, P.,
361   Satheesh, S. K., Sherwood, S., Stevens, B., and Zhang, X. Y.: Clouds and Aerosols, in: Climate Change 2013: The Physical Science
362   Basis. Contribution of Working Group I to the Fifth Assessment Report of the Intergovernmental Panel on Climate Change, edited
363   by: Stocker, T. F., Qin, D., Plattner, G.-K., Tignor, M., Allen, S. K., Boschung, J., Nauels, A., Xia, Y., Bex, V., and Midgley, P. M.,
364   Cambridge University Press, Cambridge, United Kingdom and New York, NY, USA, 571–658, 2013.
365 Capaldo, K., Corbett, J. J., Kasibhatla, P., Fischbeck, P., and Pandis, S. N.: Effects of ship emissions on sulphur cycling and radiative climate
366   forcing over the ocean, Nature, 400, 743-746, 1999.
367 Corbett, J. J., and Koehler, H. W.: Updated emissions from ocean shipping, J Geophys Res-Atmos, 108, 2003.
368 Dentener, F., Kinne, S., Bond, T., Boucher, O., Cofala, J., Generoso, S., Ginoux, P., Gong, S., Hoelzemann, J. J., Ito, A., Marelli, L., Penner, J.
369   E., Putaud, J. P., Textor, C., Schulz, M., van der Werf, G. R., and Wilson, J.: Emissions of primary aerosol and precursor gases in the
370   years 2000 and 1750 prescribed data-sets for AeroCom, Atmos Chem Phys, 6, 4321-4344, 2006.
371 Devasthale, A., Kruger, O., and Grassl, H.: Impact of ship emissions on cloud properties over coastal areas, Geophys Res Lett, 33, 2006.
372 Endresen, O., Sorgard, E., Sundet, J. K., Dalsoren, S. B., Isaksen, I. S. A., Berglen, T. F., and Gravir, G.: Emission from international sea
373   transportation and environmental impact, J Geophys Res-Atmos, 108, 2003.
374 Endresen, O., Bakke, J., Sorgard, E., Berglen, T. F., and Holmvang, P.: Improved modelling of ship SO2 emissions - a fuel-based approach,
375   Atmos Environ, 39, 3621-3628, 2005.
376 Eyring, V., Isaksen, I. S. A., Berntsen, T., Collins, W. J., Corbett, J. J., Endresen, O., Grainger, R. G., Moldanova, J., Schlager, H., and
377   Stevenson, D. S.: Transport impacts on atmosphere and climate: Shipping, Atmos Environ, 44, 4735-4771, 2010.
378 Gettelman, A., Liu, X., Ghan, S. J., Morrison, H., Park, S., Conley, A. J., Klein, S. A., Boyle, J., Mitchell, D. L., and Li, J. L. F.: Global
379   simulations of ice nucleation and ice supersaturation with an improved cloud scheme in the Community Atmosphere Model, J
380   Geophys Res-Atmos, 115, 2010.
381 Grandey, B. S., and Wang, C.: Enhanced marine sulphur emissions offset global warming and impact rainfall, Scientific Reports, 5, 2015.
382 Grandey, B. S., Rothenberg, D., Avramov, A., Jin, Q., Lee, H.-H., Liu, X., Lu, Z., Albani, S., and Wang, C.: Effective radiative forcing in the
383   aerosol–climate model CAM5.3-MARC-ARG, Atmos Chem Phys, 18, 15783-15810, 10.5194/acp-18-15783-2018, 2018.
384 Gunson, J. R., Spall, S. A., Anderson, T. R., Jones, A., Totterdell, I. J., and Woodage, M. J.: Climate sensitivity to ocean dimethylsulphide
385   emissions, Geophys Res Lett, 33, 2006.
386 International Maritime Organization: IMO sets 2020 date for ships to comply with low sulphur fuel oil requirement,
387   http://www.imo.org/en/MediaCentre/PressBriefings/Pages/MEPC-70-2020sulphur.aspx, 2016.
388 Kawecki, S., and Steiner, A. L.: The Influence of Aerosol Hygroscopicity on Precipitation Intensity During a Mesoscale Convective Event, J
389   Geophys Res-Atmos, 123, 424-442, 2018.
390 Kim, D., Wang, C., Ekman, A. M. L., Barth, M. C., and Rasch, P. J.: Distribution and direct radiative forcing of carbonaceous and sulfate
391   aerosols in an interactive size-resolving aerosol-climate model, J Geophys Res-Atmos, 113, 2008.

Kim, D., Wang, C., Ekman, A. M. L., Barth, M. C., and Lee, D. I.: The responses of cloudiness to the direct radiative effect of sulfate and carbonaceous aerosols, J Geophys Res-Atmos, 119, 1172-1185, 2014.

Klein, S. A., and Hartmann, D. L.: The Seasonal Cycle of Low Stratiform Clouds, Journal of Climate, 6, 1587-1606, 1993.

Klimont, Z., Smith, S. J., and Cofala, J.: The last decade of global anthropogenic sulfur dioxide: 2000-2011 emissions, Environ Res Lett, 8, 2013.

Lauer, A., Eyring, V., Hendricks, J., Jockel, P., and Lohmann, U.: Global model simulations of the impact of ocean-going ships on aerosols, clouds, and the radiation budget, Atmos Chem Phys, 7, 5061-5079, 2007.

Lauer, A., Eyring, V., Corbett, J. J., Wang, C. F., and Winebrake, J. J.: Assessment of Near-Future Policy Instruments for Oceangoing Shipping: Impact on Atmospheric Aerosol Burdens and the Earth's Radiation Budget, Environ Sci Technol, 43, 5592-5598, 2009.

Liu, X., Easter, R. C., Ghan, S. J., Zaveri, R., Rasch, P., Shi, X., Lamarque, J. F., Gettelman, A., Morrison, H., Vitt, F., Conley, A., Park, S., Neale, R., Hannay, C., Ekman, A. M. L., Hess, P., Mahowald, N., Collins, W., Iacono, M. J., Bretherton, C. S., Flanner, M. G., and Mitchell, D.: Toward a minimal representation of aerosols in climate models: description and evaluation in the Community Atmosphere Model CAM5, Geosci Model Dev, 5, 709-739, 2012.

Mahajan, A. S., Fadnavis, S., Thomas, M. A., Pozzoli, L., Gupta, S., Royer, S. J., Saiz-Lopez, A., and Simo, R.: Quantifying the impacts of an updated global dimethyl sulfide climatology on cloud microphysics and aerosol radiative forcing, J Geophys Res-Atmos, 120, 2524-2536, 2015.

Mahowald, N. M., Muhs, D. R., Levis, S., Rasch, P. J., Yoshioka, M., Zender, C. S., and Luo, C.: Change in atmospheric mineral aerosols in response to climate: Last glacial period, preindustrial, modern, and doubled carbon dioxide climates, J Geophys Res-Atmos, 111, 2006.

Malavelle, F. F., Haywood, J. M., Jones, A., Gettelman, A., Clarisse, L., Bauduin, S., Allan, R. P., Karset, I. H. H., Kristjansson, J. E., Oreopoulos, L., Cho, N., Lee, D., Bellouin, N., Boucher, O., Grosvenor, D. P., Carslaw, K. S., Dhomse, S., Mann, G. W., Schmidt, A., Coe, H., Hartley, M. E., Dalvi, M., Hill, A. A., Johnson, B. T., Johnson, C. E., Knight, J. R., O'Connor, F. M., Partridge, D. G., Stier, P., Myhre, G., Platnick, S., Stephens, G. L., Takahashi, H., and Thordarson, T.: Strong constraints on aerosol-cloud interactions from volcanic eruptions, Nature, 546, 485-491, 10.1038/nature22974, 2017.

McCoy, D. T., Burrows, S. M. W., Robert,, Grosvenor, D. P., Elliott, S. M., Ma, P.-L., Rasch, P. J., and Hartmann, D. L.: Natural aerosols explain seasonal and spatial patterns of Southern Ocean cloud albedo, 1, 10.1126/sciadv.1500157, 2015.

Morrison, H., and Gettelman, A.: A new two-moment bulk stratiform cloud microphysics scheme in the community atmosphere model, version 3 (CAM3). Part I: Description and numerical tests, Journal of Climate, 21, 3642-3659, 2008.

Neubauer, D., Lohmann, U., Hoose, C., and Frontoso, M. G.: Impact of the representation of marine stratocumulus clouds on the anthropogenic aerosol effect, Atmos Chem Phys, 14, 11997-12022, 2014.

Notteboom, T.: The impact of low sulphur fuel requirements in shipping on the competitiveness of roro shipping in Northern Europe, WMU Journal of Maritime Affairs, 10, 63-95, 10.1007/s13437-010-0001-7, 2010.

Pandis, S. N., Russell, L. M., and Seinfeld, J. H.: The Relationship between Dms Flux and Ccn Concentration in Remote Marine Regions, J Geophys Res-Atmos, 99, 16945-16957, 1994.

Partanen, A. I., Laakso, A., Schmidt, A., Kokkola, H., Kuokkanen, T., Pietikainen, J. P., Kerminen, V. M., Lehtinen, K. E. J., Laakso, L., and Korhonen, H.: Climate and air quality trade-offs in altering ship fuel sulfur content, Atmos Chem Phys, 13, 12059-12071, 2013.

Peters, K., Stier, P., Quaas, J., and Grassl, H.: Aerosol indirect effects from shipping emissions: sensitivity studies with the global aerosol-climate model ECHAM-HAM, Atmos Chem Phys, 12, 5985-6007, 2012.

Peters, K., Stier, P., Quaas, J., and Grassl, H.: Corrigendum to "Aerosol indirect effects from shipping emissions: sensitivity studies with the global aerosol-climate model ECHAM-HAM" published in Atmos. Chem. Phys., 12, 5985–6007, 2012, Atmos Chem Phys, 13, 6429-6430, 10.5194/acp-13-6429-2013, 2013.

Peters, K., Quaas, J., Stier, P., and Graßl, H.: Processes limiting the emergence of detectable aerosol indirect effects on tropical warm clouds in global aerosol-climate model and satellite data, Tellus B: Chemical and Physical Meteorology, 66, 24054, 10.3402/tellusb.v66.24054, 2014.

Possner, A., Zubler, E., Lohmann, U., and Schär, C.: The resolution dependence of cloud effects and ship-induced aerosol-cloud interactions in marine stratocumulus, Journal of Geophysical Research: Atmospheres, 121, 4810-4829, 10.1002/2015jd024685, 2016.

Pringle, K. J., Tost, H., Pozzer, A., Pöschl, U., and Lelieveld, J.: Global distribution of the effective aerosol hygroscopicity parameter for CCN activation, Atmos Chem Phys, 10, 5241-5255, 10.5194/acp-10-5241-2010, 2010.

Quinn, P. K., Bates, T. S., Covert, D. S., Ramsey-Bell, D. C., and McInnes, L.: Dimethylsulphide: Oceans, Atmosphere and Climate, in: Air Pollution Research Reports, 1 ed., edited by: Restelli, G., and Angeletti, G., 43, Springer Netherlands, 400, 1993.

Righi, M., Klinger, C., Eyring, V., Hendricks, J., Lauer, A., and Petzold, A.: Climate Impact of Biofuels in Shipping: Global Model Studies of the Aerosol Indirect Effect, Environ Sci Technol, 45, 3519-3525, 2011.

Rothenberg, D., and Wang, C.: Metamodeling of Droplet Activation for Global Climate Models, J Atmos Sci, 73, 1255-1272, 2016.

Rothenberg, D., and Wang, C.: An aerosol activation metamodel of v1.2.0 of the pyrcel cloud parcel model: development and offline assessment for use in an aerosol-climate model, Geosci Model Dev, 10, 1817-1833, 2017.

Rothenberg, D., Avramov, A., and Wang, C.: On the representation of aerosol activation and its influence on model-derived estimates of the aerosol indirect effect, Atmos Chem Phys, 18, 7961-7983, 10.5194/acp-18-7961-2018, 2018.

Russell, L. M., Pandis, S. N., and Seinfeld, J. H.: Aerosol Production and Growth in the Marine Boundary-Layer, J Geophys Res-Atmos, 99, 20989-21003, 1994.

Scanza, R. A., Mahowald, N., Ghan, S., Zender, C. S., Kok, J. F., Liu, X., Zhang, Y., and Albani, S.: Modeling dust as component minerals in the Community Atmosphere Model: development of framework and impact on radiative forcing, Atmos Chem Phys, 15, 537-561, 2015.

Schreier, M., Mannstein, H., Eyring, V., and Bovensmann, H.: Global ship track distribution and radiative forcing from 1 year of AATSR data, Geophys Res Lett, 34, 2007.

Tesdal, J. E., Christian, J. R., Monahan, A. H., and von Salzen, K.: Sensitivity of modelled sulfate aerosol and its radiative effect on climate to ocean DMS concentration and air-sea flux, Atmos Chem Phys, 16, 10847-10864, 2016.

458   Thomas, M. A., Suntharalingam, P., Pozzoli, L., Rast, S., Devasthale, A., Kloster, S., Feichter, J., and Lenton, T. M.: Quantification of DMS
459   aerosol-cloud-climate interactions using the ECHAM5-HAMMOZ model in a current climate scenario, Atmos Chem Phys, 10, 7425-
460   7438, 2010.
461   Thomas, M. A., Suntharalingam, P., Pozzoli, L., Devasthale, A., Kloster, S., Rast, S., Feichter, J., and Lenton, T. M.: Rate of non-linearity in
462   DMS aerosol-cloud-climate interactions, Atmos Chem Phys, 11, 11175-11183, 2011.
463   Warren, S. G., Hahn, C. J., London, J. , Chervin, R. M., and Jenne, R. L.: Global Distribution of Total Cloud Cover and Cloud Type Amounts
464   Over Ocean, NCAR Technical Note NCAR/TN-273+STR, doi:10.5065/D6GH9FXB, 1988.
465   Winebrake, J. J., Corbett, J. J., Green, E. H., Lauer, A., and Eyring, V.: Mitigating the Health Impacts of Pollution from Oceangoing Shipping:
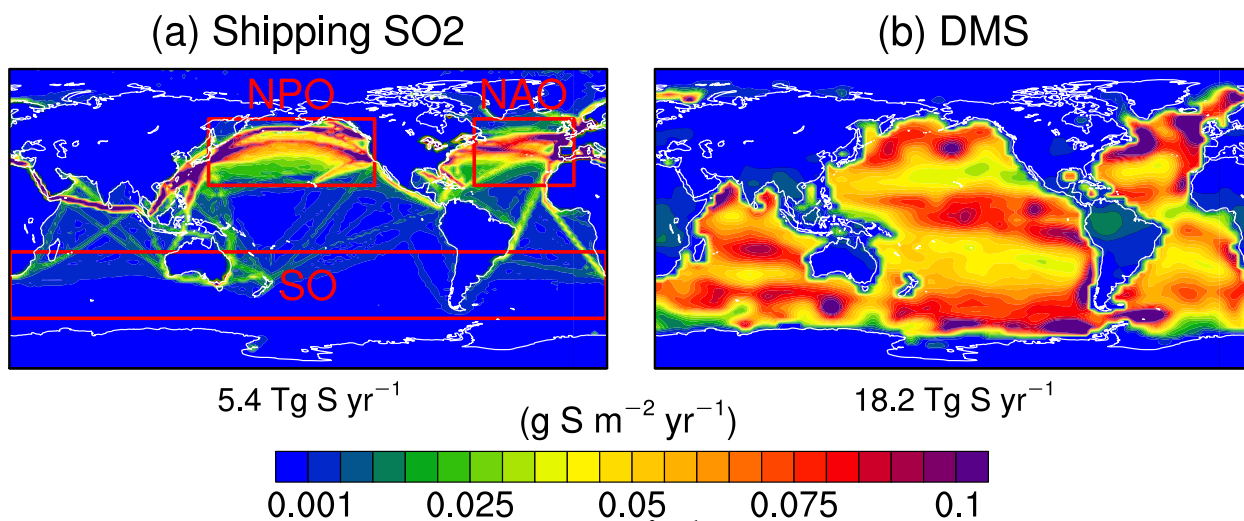466   An Assessment of Low-Sulfur Fuel Mandates, Environ Sci Technol, 43, 4776-4782, 2009.
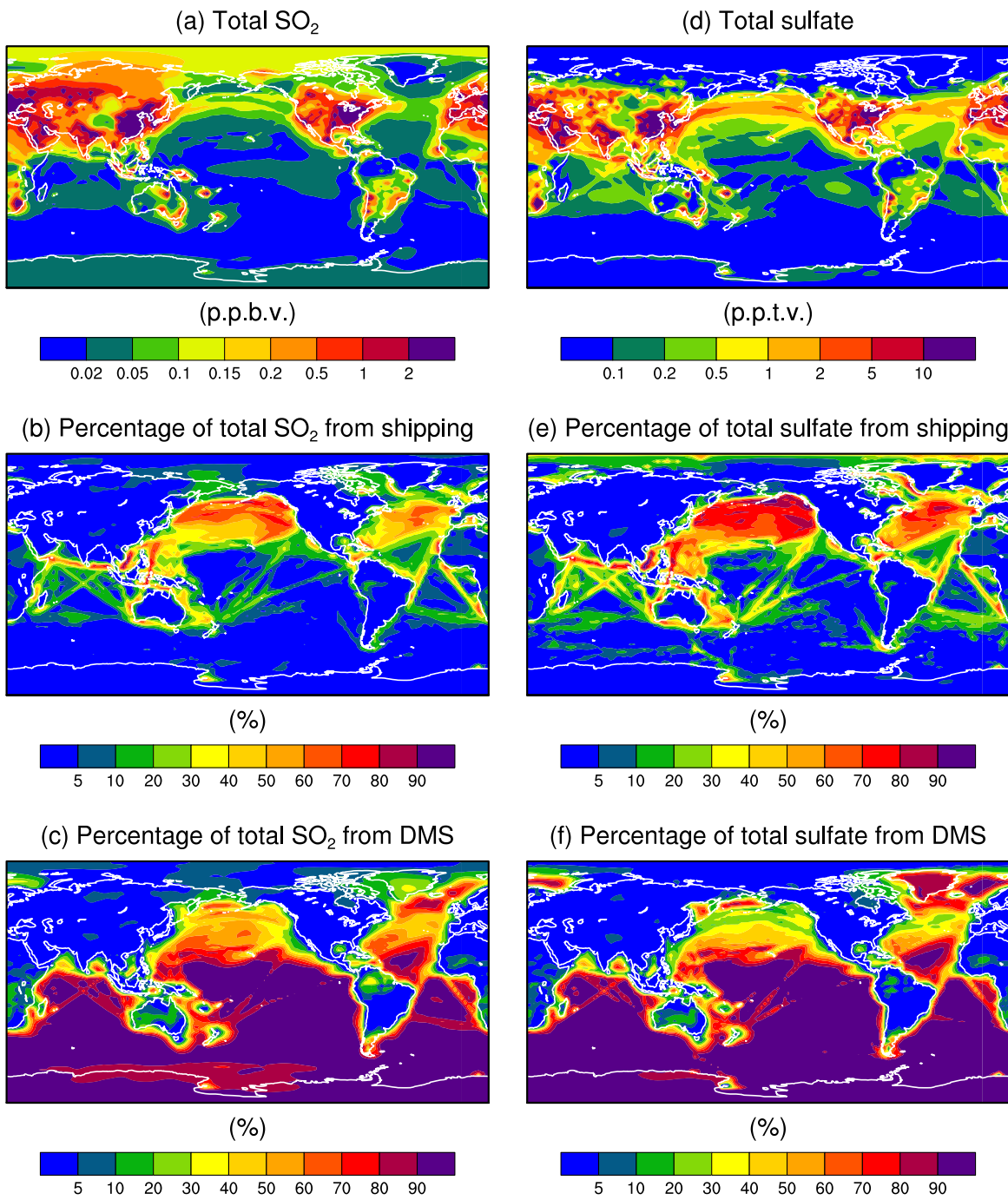467

468   **Table 1. Summary of experiments.**

Aerosol Modules	Experiments	DMS emissions	Ship emissions	Description
MARC	Shipping	DMSRef	*ShipZero*	DMS emission (Tg S yr^{-1}):
			ShipLow	DMSZero: 0
			ShipRef	DMSLow: 9.1
			ShipHigh	DMSRef: 18.2
	DMS	*DMSZero*	*ShipZero*	
			ShipRef	
		DMSLow	*ShipZero*	
			ShipRef	Ship emission (Tg S yr^{-1}):
MAM3	DMS	*DMSRef*	*ShipZero*	ShipZero: 0
			ShipRef	ShipLow: 1.0 (0.5%)
		DMSZero	*ShipZero*	ShipRef: 5.4(2.7%)
			ShipRef	ShipHigh: 7.0 (3.5%)
		DMSLow	*ShipZero*	
			ShipRef	

469   Notes: in *ShipZero* experiments, emission rates of all gas-phase and aerosol species from shipping emissions are set to zero;
470   while in *ShipLow*, *ShipRef*, and *ShipHigh* experiments, all shipping emission rates (such as OC and BC) are set to year-2000
471   values except for emission rates of sulfur compounds (i.e. SO_2 and SO_4) which are modified. The percent for ship emission in the
472   last column stands for the proportion of sulfur content in the heavy fuel oils by mass.

473

(a) Shipping SO2   **(b) DMS**

5.4 Tg S yr^{-1} 18.2 Tg S yr^{-1}

(g S m^{-2} yr^{-1})

0.001   0.025   0.05   0.075   0.1

474
475   **Figure 1. Spatial patterns of annual means of sulfur emission (g S m^{-2} yr^{-1}) from (a) international shipping and (b) natural DMS in the**
476   **simulation at the reference emission level (i.e., *ShipRef_DMSRef*). The numbers below each panel are the global total annual emissions.**
477   **Three regions are selected for further analysis: The North Pacific Ocean (NPO; 20°N–60°N, 140°E–240°E), the North Atlantic Ocean**
478   **(NAO; 20°N–60°N, 300°E–360°E), and the Southern Ocean (SO; 20°S–60°S, 0°E–360°E).**

(a) Total SO$_2$

(d) Total sulfate

(p.p.b.v.)

(p.p.t.v.)

(b) Percentage of total SO$_2$ from shipping

(e) Percentage of total sulfate from shipping

(%)

(%)

(c) Percentage of total SO$_2$ from DMS
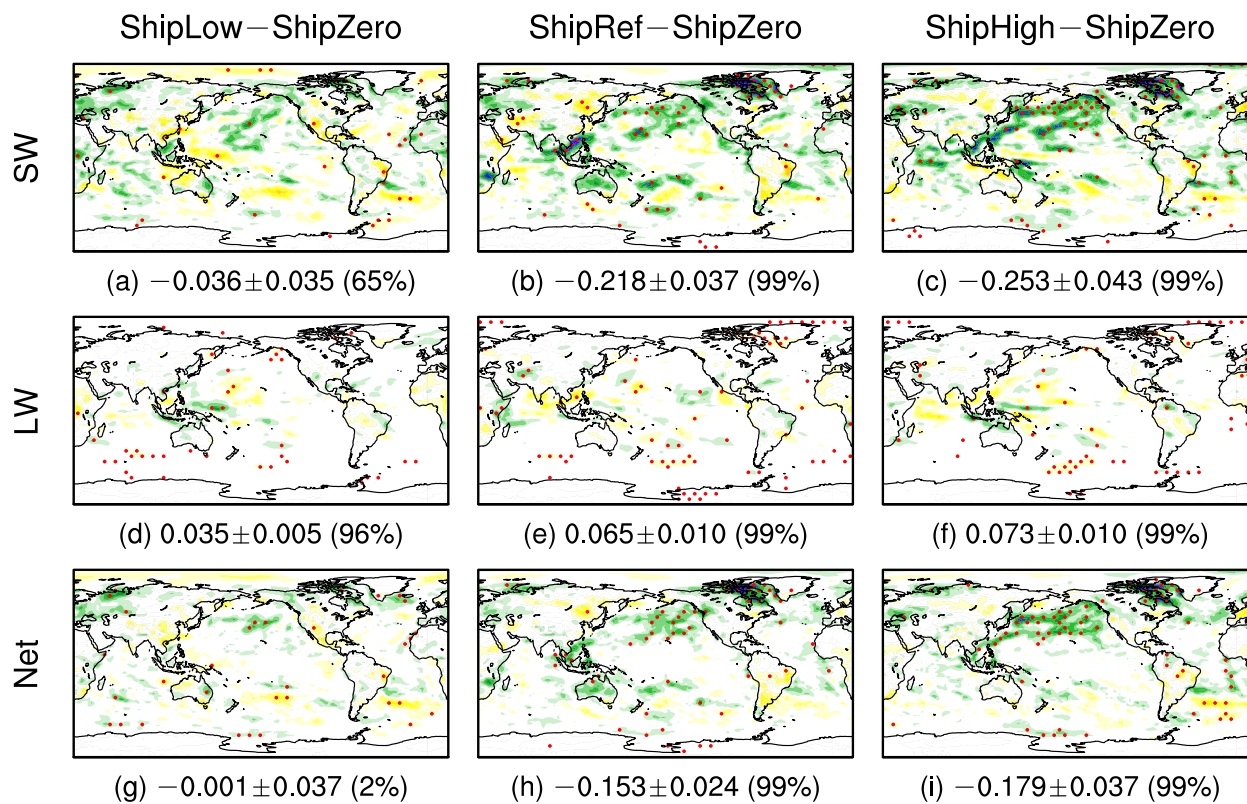
(f) Percentage of total sulfate from DMS

(%)

(%)

479
480 **Figure 2. Spatial patterns of (a) annual mean concentrations of total SO₂ (units: parts per billion by volume; ppbv), (b) and (c) are**
481 **respectively the contributions of shipping emission and natural DMS to total SO₂ in the lowest model layer. (d)–(f) are the same as (a)–**
482 **(c), but for sulfate aerosols. These results are from MARC simulations and calculated as the differences between the simulations with**
483 **the international shipping and DMS emissions at the reference and zero levels (i.e., *ShipRef_DMSRef* minus *ShipZero_DMSRef* and**
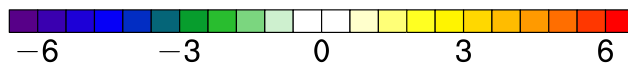484 ***ShipRef_DMSRef* minus *ShipRef_DMSZero*).**
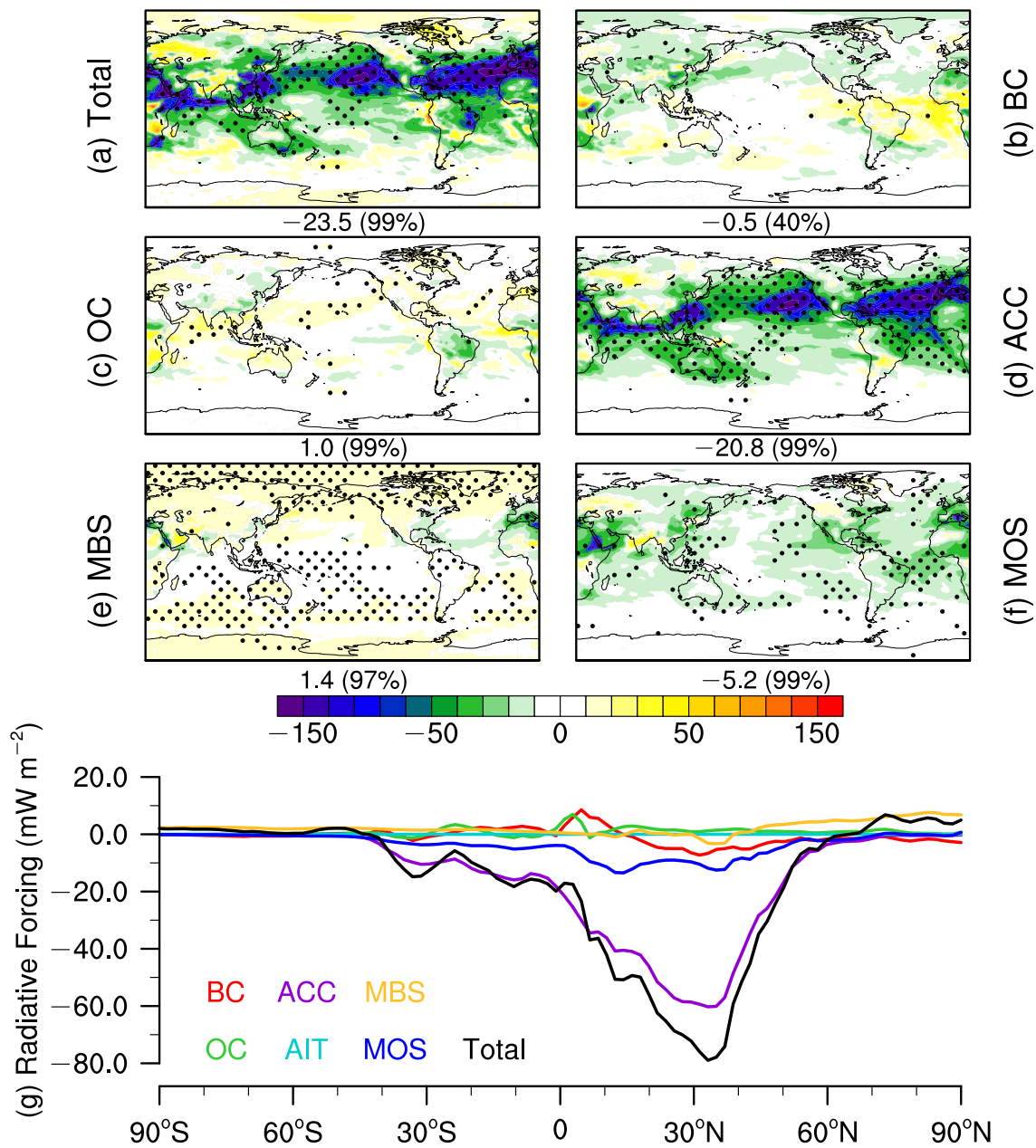
Figure 3. Simulated direct radiative effect (DRE; units: mW m^{-2}) of ISE at TOA by MARC. The DRE is calculated as the difference between simulation results with and without ISE (i.e., *ShipRef_DMSRef* minus *ShipZero_DMSRef*) and averaged over the 30-year period of simulations at all-sky conditions. Panels (a)–(f) show the spatial patterns of DRE due to ISE with the global mean differences and the associated significant levels indicated by the numbers bellow each panel and panel (g) is the meridional variations of zonal mean DRE for various aerosol types from ISE and their total effects. The expansions of the abbreviations can be found in Section 2.3. The black dots represent grid points that are statistically significant above the 90% confidence level based on the two-tailed Student's *t*-test.

15

DMSRef

| ShipLow−ShipZero | ShipRef−ShipZero | ShipHigh−ShipZero |

SW

(a) −0.036±0.035 (65%)   (b) −0.218±0.037 (99%)   (c) −0.253±0.043 (99%)

LW

(d) 0.035±0.005 (96%)   (e) 0.065±0.010 (99%)   (f) 0.073±0.010 (99%)

Net

(g) −0.001±0.037 (2%)   (h) −0.153±0.024 (99%)   (i) −0.179±0.037 (99%)

Cloud radiative effect at TOA (W m^{-2})

−6   −3   0   3   6

Figure 4. Spatial patterns of MARC simulated cloud radiative effect (CRE; units: W m^{-2}) at TOA of ISE with various shipping emission levels. The CRE is calculated as the differences of radiation flux at TOA and at all-sky conditions between the simulation without shipping emissions and three simulations with the same DMS emissions at the reference level but various shipping emission levels (i.e., low, reference, high) in short-wave (SW), long-wave (LW), and net (SW+LW) and averaged over the 30-year simulation period. The numbers below each panel are the global means, standard deviation across the 30-year period, and the confidence level. The red dots represent grid points that are statistically significant above the 90% confidence level based on the two-tailed Student's *t*-test.

DMSRef

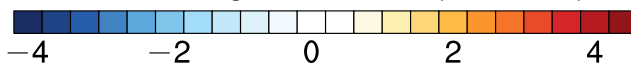ShipLow−ShipZero   ShipRef−ShipZero   ShipHigh−ShipZero
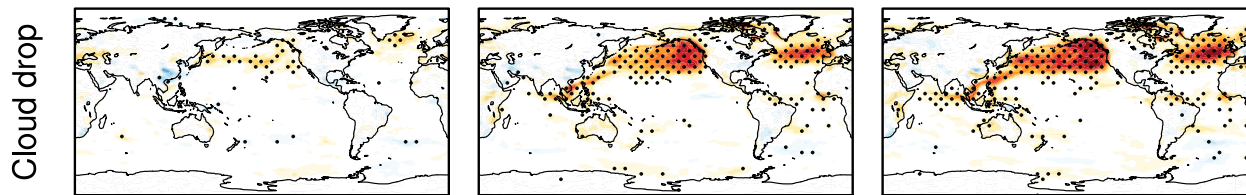
Cloud drop

(a) 0.037±0.011 (91%)   (b) 0.305±0.009 (99%)   (c) 0.406±0.013 (99%)

Column-integrated cloud # ($\times 10^9$ m^{-2})

−4   −2   0   2   4

Figure 5. Spatial patterns of MARC simulated column-integrated cloud droplet number concentration ($\times 10^9$ m^{-2}) response to international shipping emissions. The responses are calculated as the differences of cloud droplet number integrated through the whole atmospheric columns between the simulation without shipping emissions and three simulations with the reference shipping emission and various DMS emissions (i.e., zero, low, and reference) over the 30-year simulation period. The numbers below each panel are the global means, standard deviation across the 30-year period, and the confidence level. The black dots represent grid points that are statistically significant above the 90% confidence level based on the two-tailed Student's *t*-test.

Figure 6. Spatial patterns of MARC simulated cloud radiative effect (CRE; units: W m^{-2}) at TOA of ISE at various DMS emission levels. The CRE is calculated as the differences of radiation flux at TOA and at all-sky conditions between the simulation without shipping emissions and three simulations with the same shipping emissions at the reference level but various DMS emission levels (i.e., zero, low, and reference) in short-wave (SW), long-wave (LW), and net (SW+LW) and averaged over the 30-year simulation period. The numbers below each panel are the global means, standard deviation across the 30-year period, and the confidence level. The black dots represent grid points that are statistically significant above the 90% confidence level based on the two-tailed Student's *t*-test.
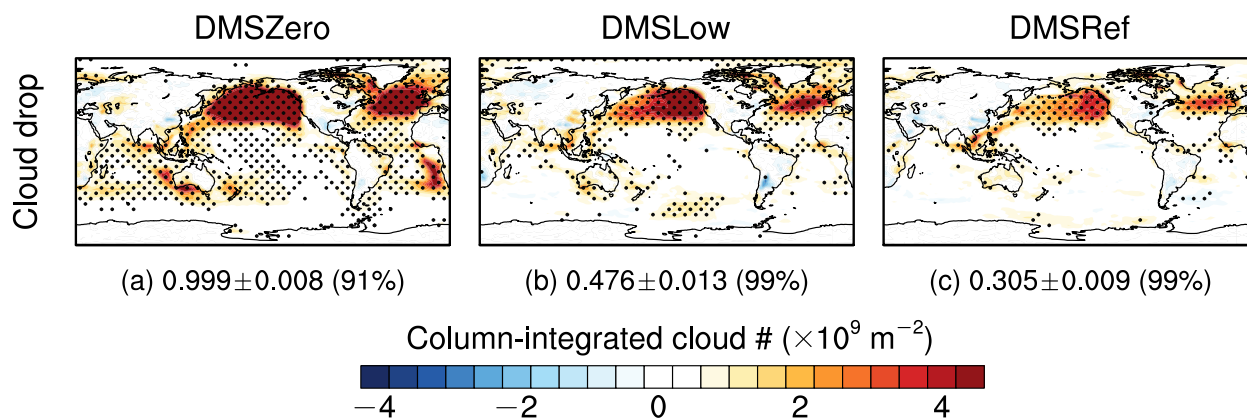
ShipRef−ShipZero
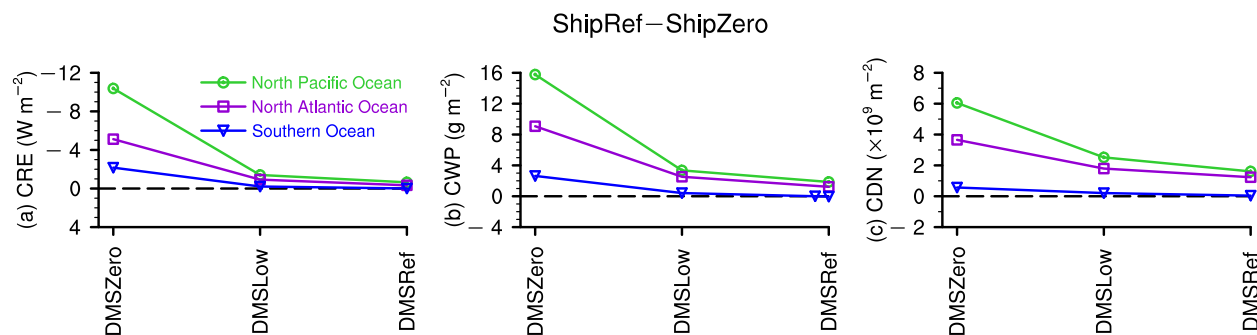
DMSZero

DMSLow

DMSRef

Cloud drop

(a) 0.999±0.008 (91%)   (b) 0.476±0.013 (99%)   (c) 0.305±0.009 (99%)

Column-integrated cloud # ($\times 10^9$ m^{-2})

−4   −2   0   2   4

Figure 7. Spatial patterns of MARC simulated column-integrated cloud droplet number concentration ($\times 10^9$ m^{-2}) response to international shipping emissions. The responses are calculated as the differences of cloud droplet number integrated through the whole atmospheric columns between the simulation without shipping emissions and three simulations with the reference shipping emission and various DMS emissions (i.e., zero, low, and reference) over the 30-year simulation period. The numbers below each panel are the global means, standard deviation across the 30-year period, and the confidence level. The black dots represent grid points that are statistically significant above the 90% confidence level based on the two-tailed Student's t-test.

ShipRef−ShipZero

Figure 8. Impacts of DMS emissions on cloud responses to international shipping emissions. (a) Cloud radiative effects at TOA (W m^{-2}), (b) column-integrated cloud water path (g m^{-2}), and (c) column-integrated cloud droplet number ($\times 10^9$ m^{-2}). The green, purple, and blue curves respectively represent quantities area-averaged over the North Pacific Ocean (NPO), the North Atlantic Ocean (NAO), and the Southern Ocean (SO), which are shown as red boxes in Figure 1a. These results are from MARC simulations.
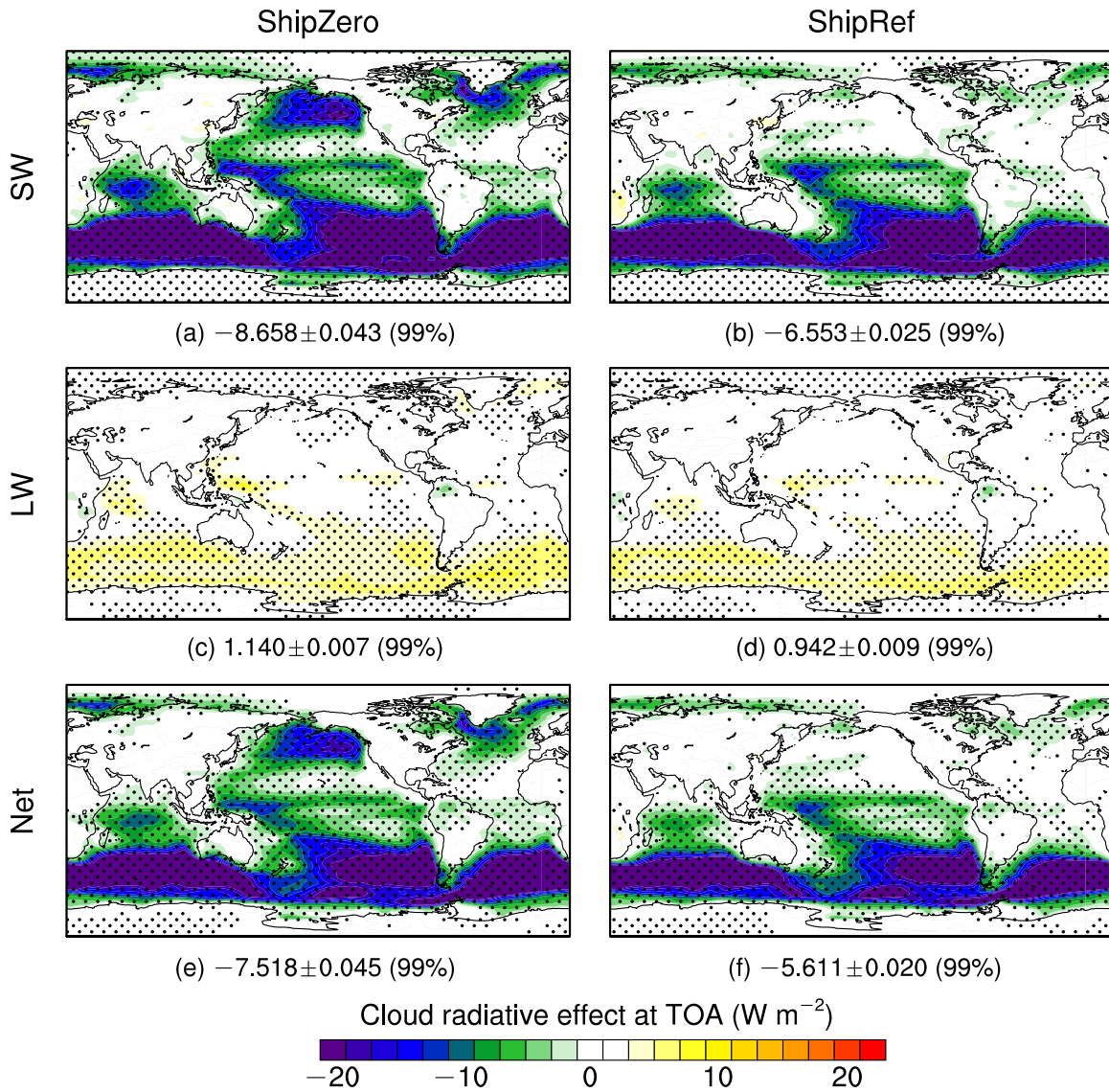
DMSRef−DMSZero

ShipZero　　　　　　　　　　　　　ShipRef

SW

(a) −8.658±0.043 (99%)　　　　　(b) −6.553±0.025 (99%)

LW

(c) 1.140±0.007 (99%)　　　　　　(d) 0.942±0.009 (99%)

Net

(e) −7.518±0.045 (99%)　　　　　(f) −5.611±0.020 (99%)

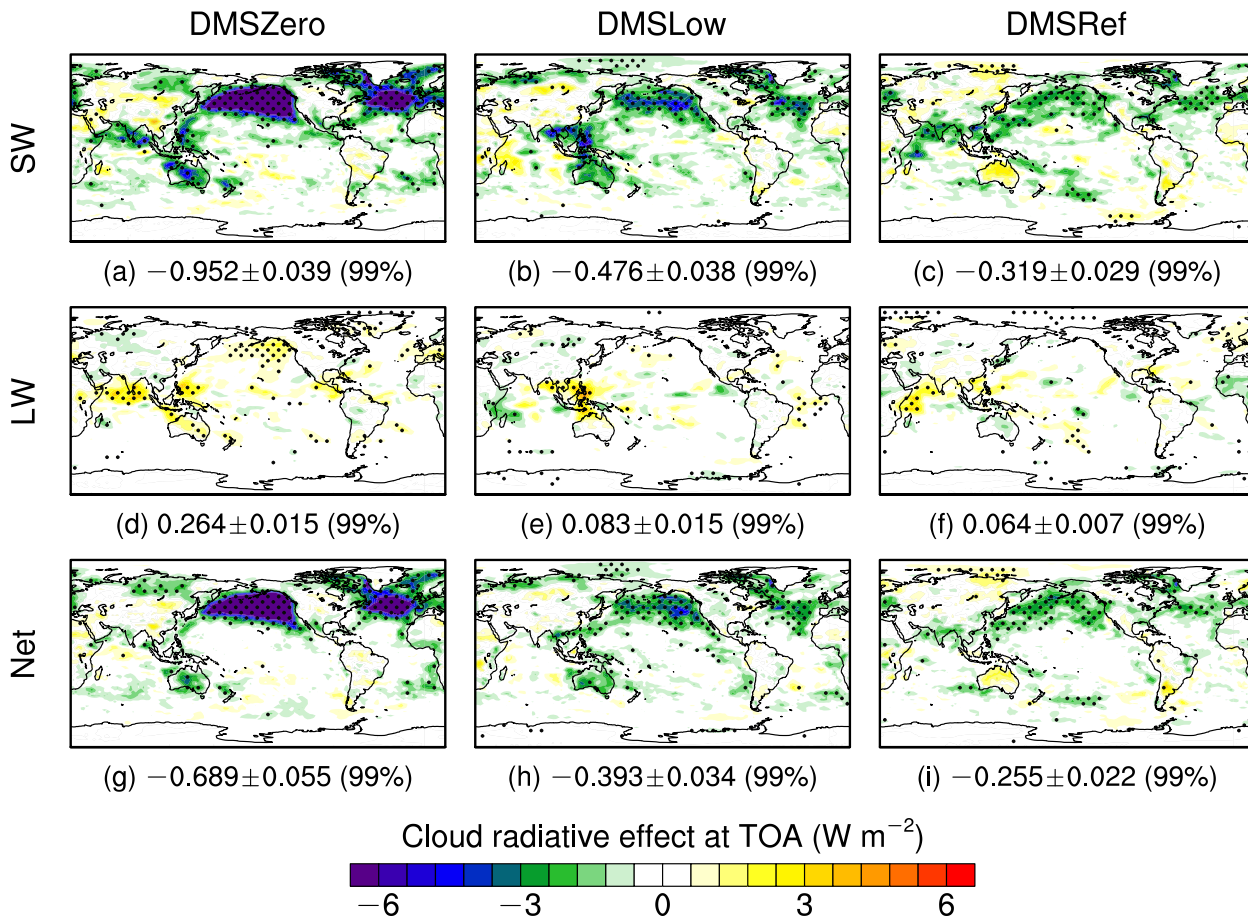Cloud radiative effect at TOA (W m^{-2})

−20　　　−10　　　0　　　10　　　20

Figure 9. Spatial patterns of MARC simulated cloud radiative effect (units: W m^{-2}) of DMS emissions at various shipping emission levels. The CRE is calculated as the differences of radiation flux at TOA and at all-sky conditions between the simulation without DMS emissions and two simulations with the same DMS emissions at the reference level but various shipping emission levels (i.e., zero and reference) in short-wave (SW), long-wave (LW), and net (SW+LW) and averaged over the 30-year simulation period. The numbers below each panel are the global means, standard deviation across the 30-year period, and the confidence level. The black dots represent grid points that are statistically significant above the 90% confidence level based on the two-tailed Student's *t*-test.

DMSRef−DMSZero
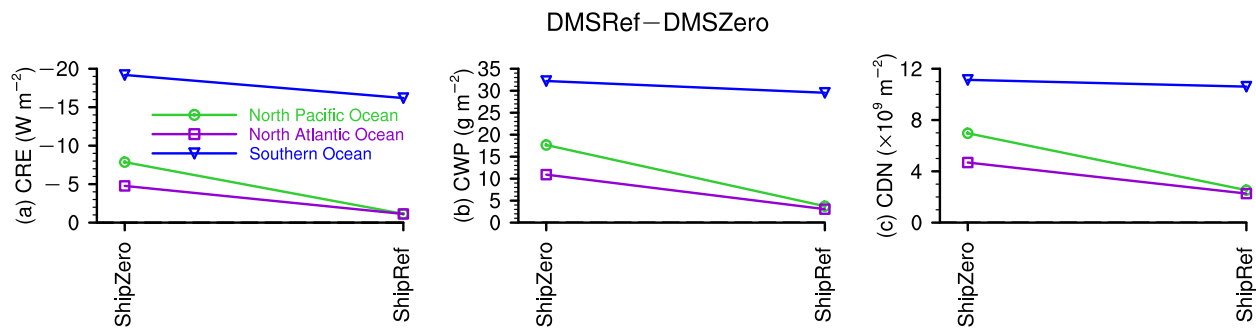
Figure 10. Impacts of ISE on cloud responses to DMS emissions. (a) Cloud radiative effects at TOA (W m^{-2}), (b) column-integrated cloud water path (g m^{-2}), and (c) column-integrated cloud droplet number (×10^9 m^{-2}). The green, purple, and blue curves respectively represent quantities area-averaged over the North Pacific Ocean (NPO), the North Atlantic Ocean (NAO), and the Southern Ocean (SO), which are shown as red boxes in Figure 1a. These results are from MARC simulations.

20

(a) −0.952±0.039 (99%)   (b) −0.476±0.038 (99%)   (c) −0.319±0.029 (99%)

(d) 0.264±0.015 (99%)   (e) 0.083±0.015 (99%)   (f) 0.064±0.007 (99%)

(g) −0.689±0.055 (99%)   (h) −0.393±0.034 (99%)   (i) −0.255±0.022 (99%)

Cloud radiative effect at TOA (W m^{-2})

572

573   **Figure 11. Same as Figure 6, but using a different aerosol module, namely MAM3 rather than MARC.**

574

575   **Figure 12. Same as Figure 8, but using a different aerosol module, namely MAM3 rather than MARC.**

21